Supplementary Fig. S1

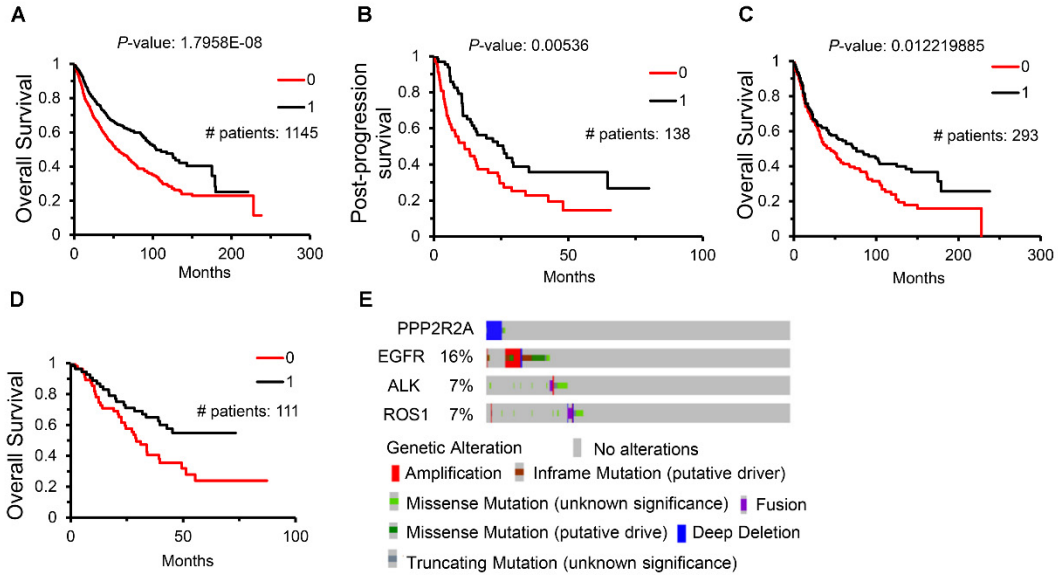

Supplementary Fig. S1. PPP2R2A deficiency is associated with poor prognosis. (A–D) Lung cancer patients with low levels of PPP2R2A have poor prognosis. Kaplan–Meier curves comparing overall (**A**) or progression-free (**B**) survival using kmplotter (kmplot.com) metadata and overall survival in GSE30219 (**C**, Rousseaux et al.; Sci Transl Med, 2013) and GSE3141 (**D**, Bild et al.; Nature, 2006). (**E**) PPP2R2A (B55α) homozygous deletion is not associated with amplification/in-frame driver mutations in EGFR, ALK, or ROS1. Mutation analysis of PPP2R2A, EGFR, ALK, and ROS1 using TCGA data. TCGA, n=507, lung adenocarcinoma.

Supplementary Fig. S2

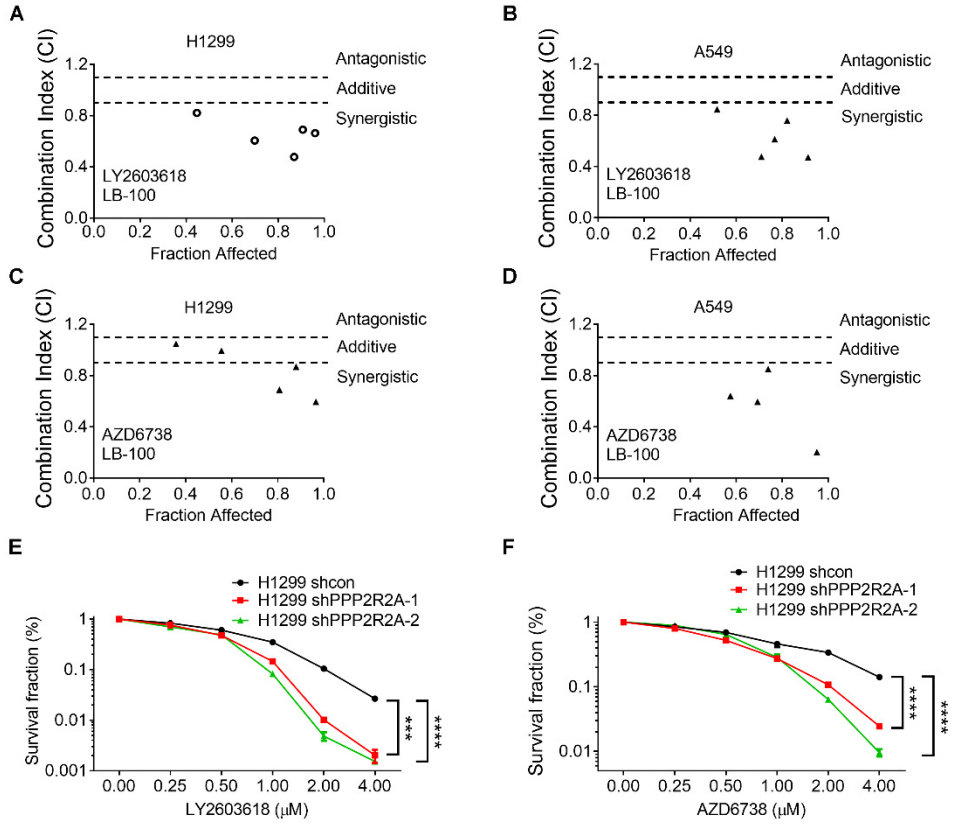

Supplementary Fig. S2. The synthetic lethality between PPP2R2A deficiency and CHK1/ATR inhibition. CHK1 inhibitor LY2603618 is synergistic with the PP2A inhibitor LB-100 in H1299 cells (**A**) and A549 cells (**C**). Similar results were found for ATR inhibition by the ATR inhibitor AZD6738 in both H1299 (**B**) and A549 (**D**) cells. Data are the means of three independent experiments. Combination indices (CIs) were calculated using the median-effect method by Compusyn. Each point represents the CI value obtained from three replicates. CI < 0.9 represents synergism, CI = 0.9–1.1 represents an additive effect, and CI > 1.1 represents antagonism. Synergist effect between loss of PPP2R2A and CHK1 inhibitor (**E**) or ATR inhibitor (**F**) in H1299 cells detected by clonogenic assay. Data are shown as the mean ± SEM of three

replicates. ***$P < 0.001$, ****$P < 0.0001$, two-way ANOVA followed by Bonferroni post-tests was used for the data analysis.

Supplementary Fig. S3

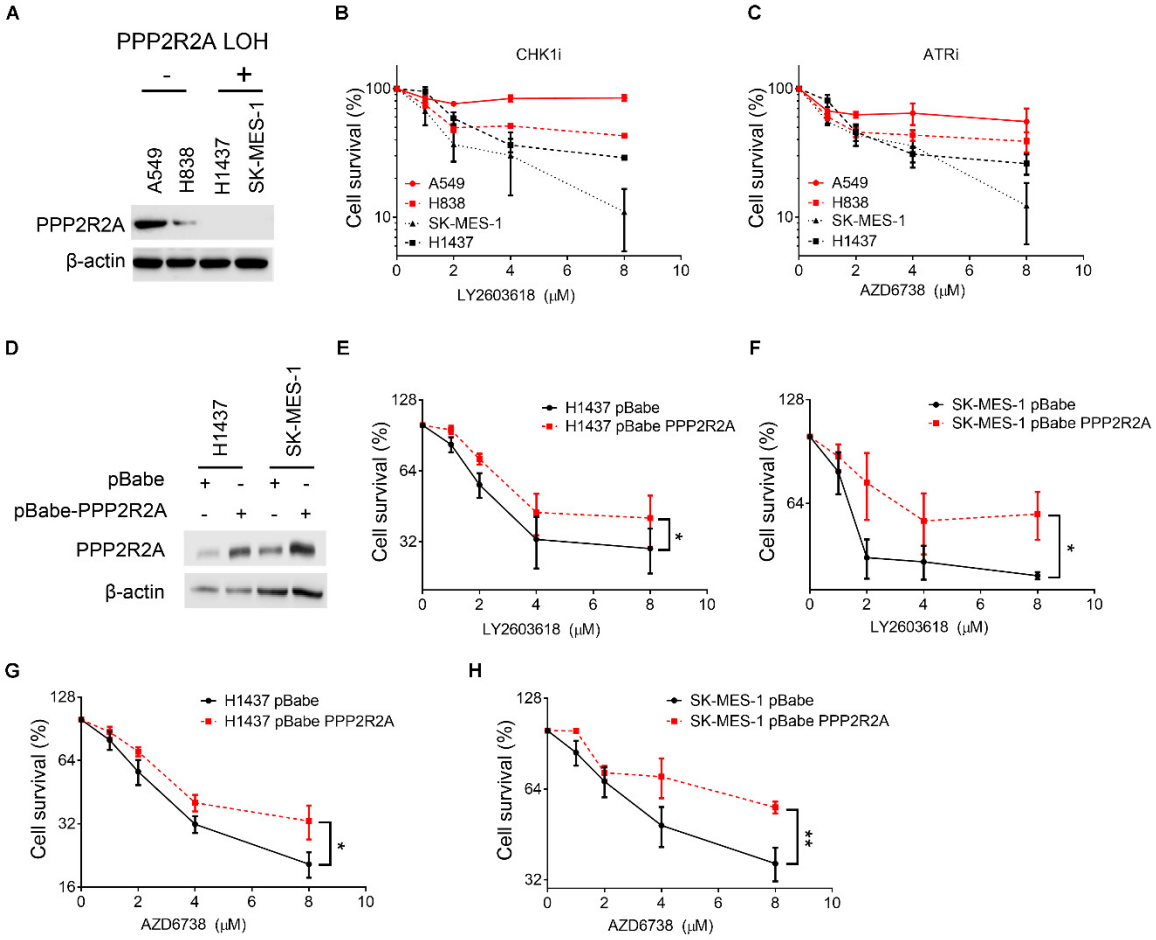

Supplementary Fig. S3. Reduced PPP2R2A expression is associated with greater sensitivity to ATR and CHK1 inhibitors. (**A**) PPP2R2A expression in the indicated NSCLC cell lines. MTT assays following CHK1 inhibition by LY2603618 (**B**) or ATR inhibition by AZD63738 (**C**) in NSCLCs with higher PPP2R2A expression (A548 and H838) versus lung cancer cells with lower PPP2R2A expression (H1437 and SK-MES-1). Cells were treated with various concentrations of LY2603618 or AZD6738 for 48 h. Data of **B** and **C** are presented as mean ± SEM of three independent experiments. Two-way ANOVA followed by Bonferroni post-tests was used for data analysis. For CHK1 inhibition: ****P < 0.0001, A549 vs. H1437; ****P < 0.0001, A549 vs. SK-MES-1; ***P < 0.001, H838 vs. SK-MES-1. For ATR inhibition: *P < 0.05, A549 vs. H1437; ***P < 0.001, A549 vs. SK-MES-1. (**D**) Overexpression of PPP2R2A protein in

NSCLC cells with loss of heterozygosity of PPP2R2A. Stable expression of PPP2R2A renders H1437 and SK-MES-1 cells less sensitive to CHK1 (**E, F**) and ATR (**G**, **H**) inhibition. Data of **E-H** are presented as mean ± SEM of three independent experiments. Significance was determined by two-way ANOVA followed by Bonferroni post-tests. *$P < 0.05$ and **$P < 0.01$.

Supplementary Fig. S4

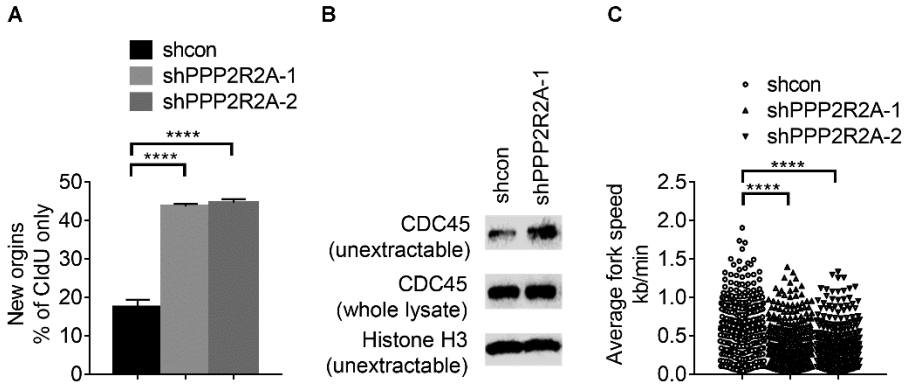

Supplementary Fig. S4. PPP2R2A knockdown increases replication initiation rate and decreases replication fork speed. (**A**) Quantification of replication initiations. PPP2R2A knockdown by shRNAs increases the rate of replication initiation in H1299 cells. (**B**) PPP2R2A deficiency increases levels of nonextractable CDC45 protein. (**C**) Analysis of average DNA fork speed in the indicated cells. PPP2R2A knockdown by shRNAs decreases replication fork speed. Data of **A** and **C** are the mean ± SEM of three independent experiments. Statistical significance was determined by one-way ANOVA followed by Bonferroni's post hoc analysis for multiple comparisons. ****$P < 0.0001$.

Supplementary Fig. S5

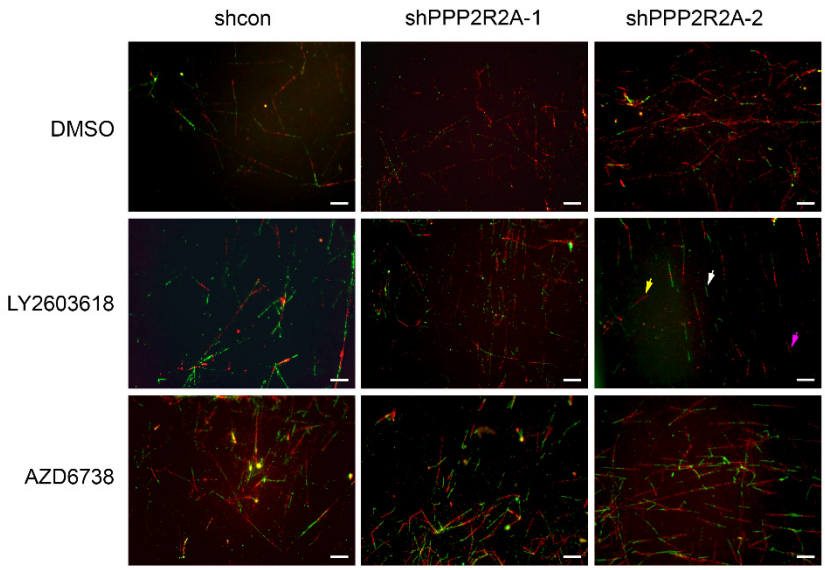

Supplementary Fig. S5. Representative images of DNA fibers from H1299 cells treated with LY2603618 (1 μM) or AZD6738 (1 μM) inhibitor. Dysregulation of replication forks is marked only in cells with PPP2R2A knockdown and CHK1 inhibition. White arrow, new replication initiation; yellow arrow, slower replication track; magenta arrow, stalled replication fork. Scale bars: 100 μm.

Supplementary Fig. S6

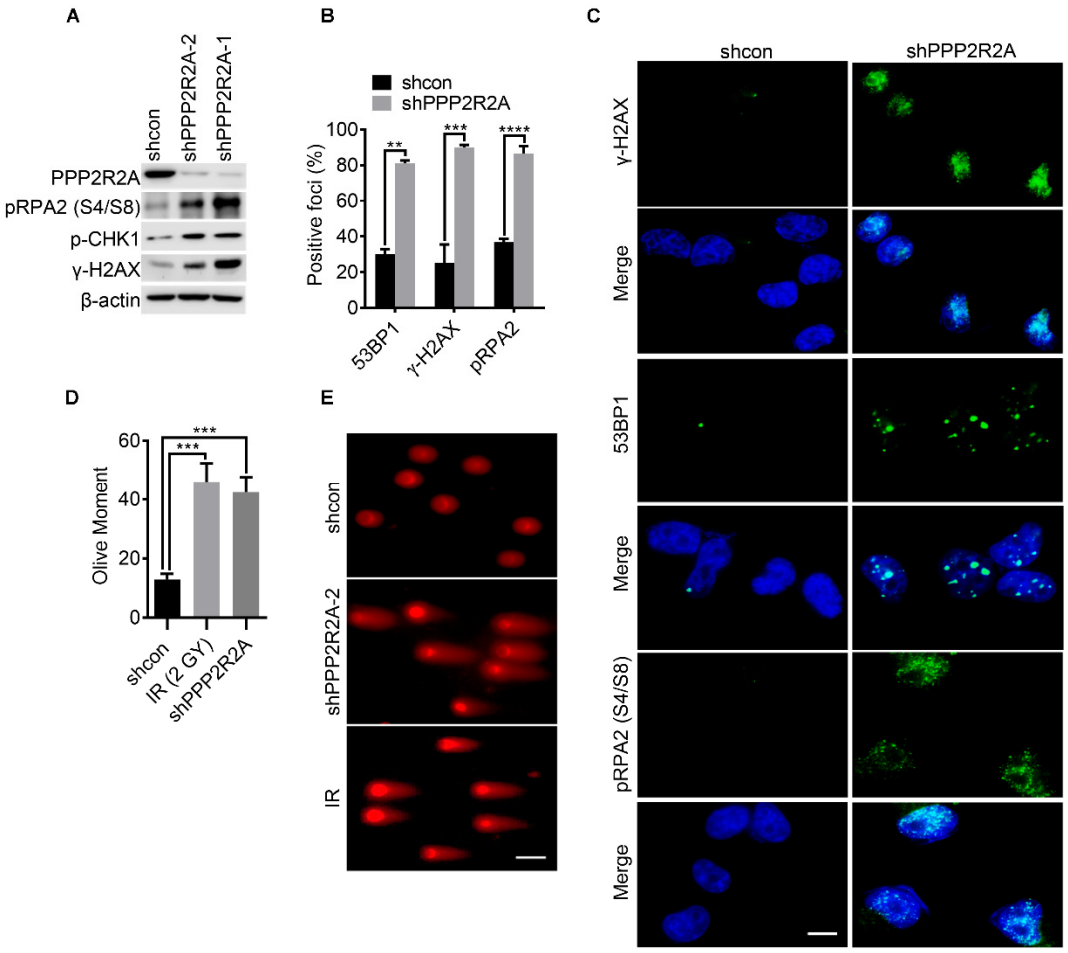

Supplementary Fig. S6. PPP2R2A knockdown leads to increased replication stress in H1299 cells. (**A**) PPP2R2A downregulation by two different shRNAs leads to increased replication stress in H1299 cells. (**B**) Loss of PPP2R2A increases the percentages of cells with positive 53BP1, γ-H2AX, and p-RPA2 foci (≥5) in H1299 cells using immunofluorescence. Data are mean ± SEM of three independent experiments. Statistical significance was determined by Student's *t* test. ***P* < 0.01, ****P* < 0.001, and *****P* < 0.0001. (**C**) Representative immunofluorescence images of γ-H2AX, 53BP1, and p-RPA2 (S4/S8) foci in H1299 cells with or without PPP2R2A knockdown. Scale bar: 100 μm. (**D**) PPP2R2A deficiency promotes DNA double-strand breaks on a Comet assay. Data are mean ± SEM of three independent

experiments. Irradiation (2 Gy) was used as a positive control. Statistical significance was determined by one-way ANOVA followed by Bonferroni's post hoc analysis for multiple comparisons. ***$P < 0.001$. (**E**) Representative immunofluorescence images used for the quantification of olive tail moment in **D**. Scale bars: 100 μm.

Supplementary Fig. S7

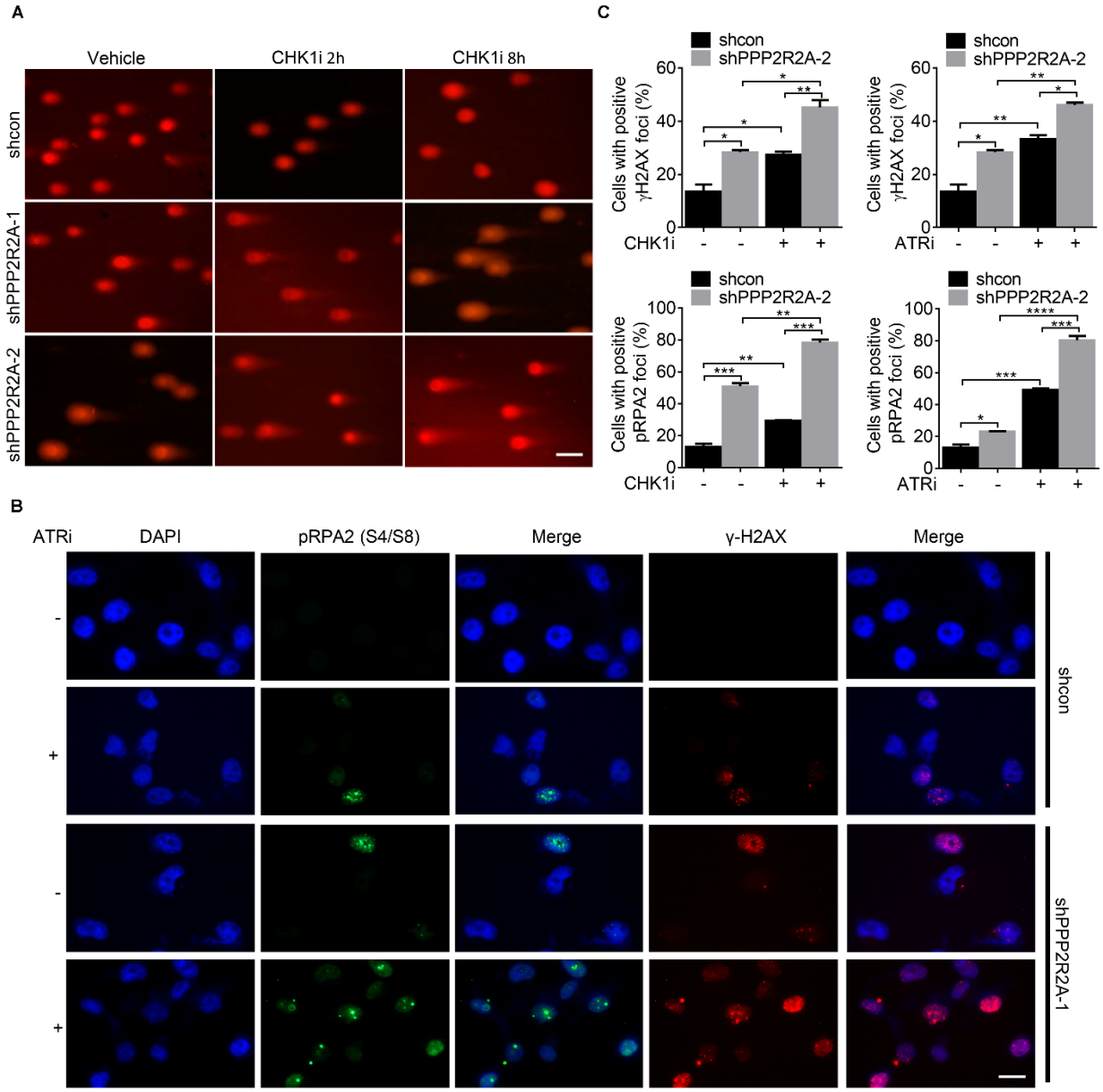

Supplementary Fig. S7. CHK1/ATR signaling inhibition promotes a replication stress increase, particularly in cells with PPP2R2A deficiency. (**A**) Loss of PPP2R2A increases DNA strand breaks in H1299 cells, as indicated by a Comet assay. Representative immunofluorescence images used for the quantification of olive tail moment. Scale bar: 100 μm. (**B**) Representative immunofluorescence images used for manual focus counting of γ-H2AX and pRPA2 (S4/S8) in H1299 control and PPP2R2A knockdown cells using shPPP2R2A-1 with or

without ATR inhibitor AZD6738 treatment (1 μM). Scale bar: 100 μm. (**C**) The percentages of H1299 control cells and PPP2R2A knockdown cells using shPPP2R2A-2 with positive γ-H2AX and p-RPA2 foci (≥5) by immunofluorescence assay. Cells were collected and fixed after LY2603618 (1 μM) or AZD6738 (1 μM) treatment for 2 h. Data are the mean ± SEM of three independent experiments. Statistical significance was determined by one-way ANOVA followed by Bonferroni's post hoc analysis for multiple comparisons. *$P < 0.05$, **$P < 0.01$, ***$P < 0.001$, and ****$P < 0.0001$.

Supplementary Fig. S8

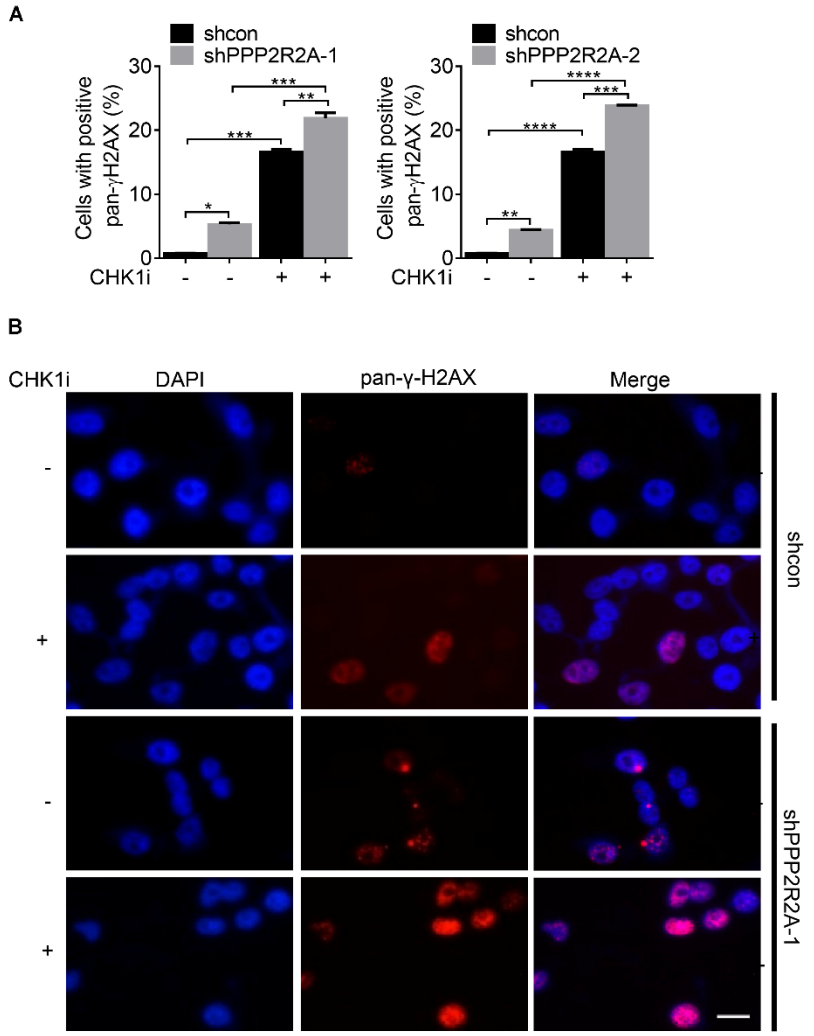

Supplementary Fig. S8. CHK1 inhibition leads to increased pan-nuclear signals of γ-H2AX, particularly in cells with reduced PPP2R2A expression. (**A**) The percentages of cells with positive pan-γ-H2AX signals in H1299 cells with or without PPP2R2A knockdown using two shRNAs. Cells were collected and fixed after treatment with CHK1 inhibitor LY2603618 (1 μM) for 2h. All data are presented as mean ± SEM. **P* < 0.05, ***P* < 0.01, ****P* < 0.001, *****P* < 0.0001, by one-way ANOVA followed by Bonferroni's post hoc test. All data are represented by three independent experiments. (**B**) Representative pictures of pan-γ-H2AX signals in H1299 cells with or without PPP2R2A knockdown in the presence or absence of CHK1 inhibition. Scale bar: 100 μm.

Supplementary Fig. S9

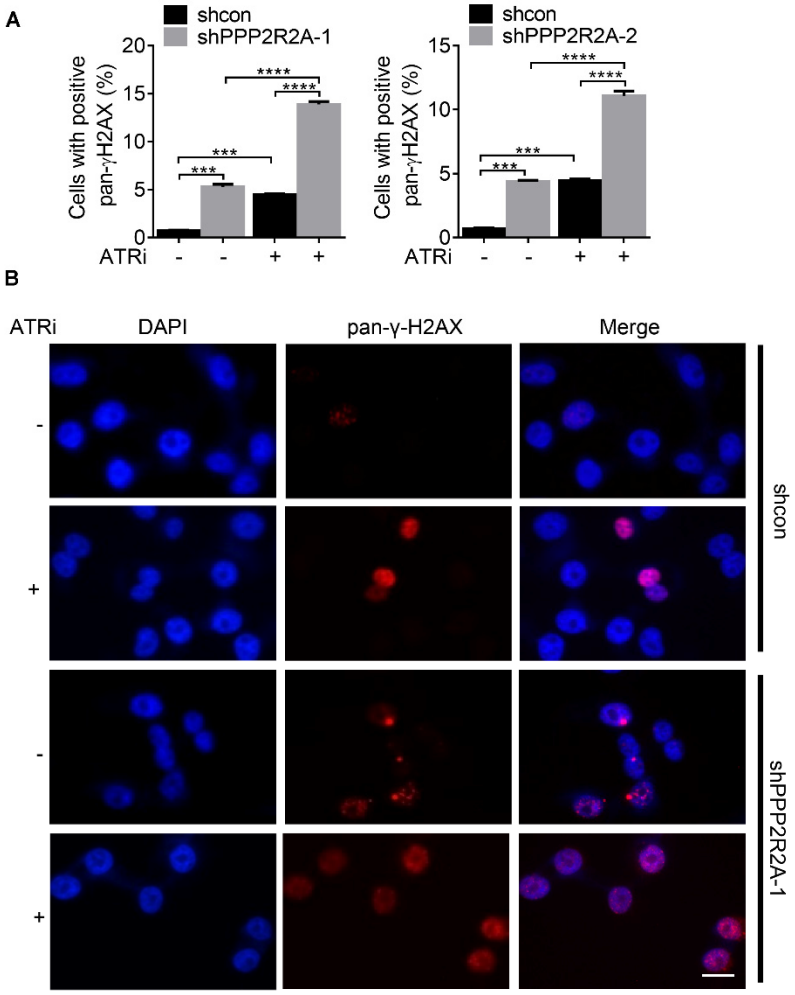

Supplementary Fig. S9. ATR inhibition leads to increased pan-nuclear signals of γ-H2AX, particularly in cells with reduced PPP2R2A expression. (**A**) The percentages of cells with positive pan-γ-H2AX signals in H1299 cells with or without PPP2R2A knockdown using two shRNAs. Cells were collected and fixed after treatment with ATR inhibitor AZD6738 (1 μM) for 2h. All data are presented as mean ± SEM. ***P < 0.001, ****P < 0.0001, by one-way ANOVA followed by Bonferroni's post hoc test. All data are represented by three independent

experiments. (**B**) Representative pictures of pan-γ-H2AX signals in H1299 cells with or without PPP2R2A knockdown in the presence or absence of ATR inhibition. Scale bar: 100 μm.

Supplementary Fig. S10

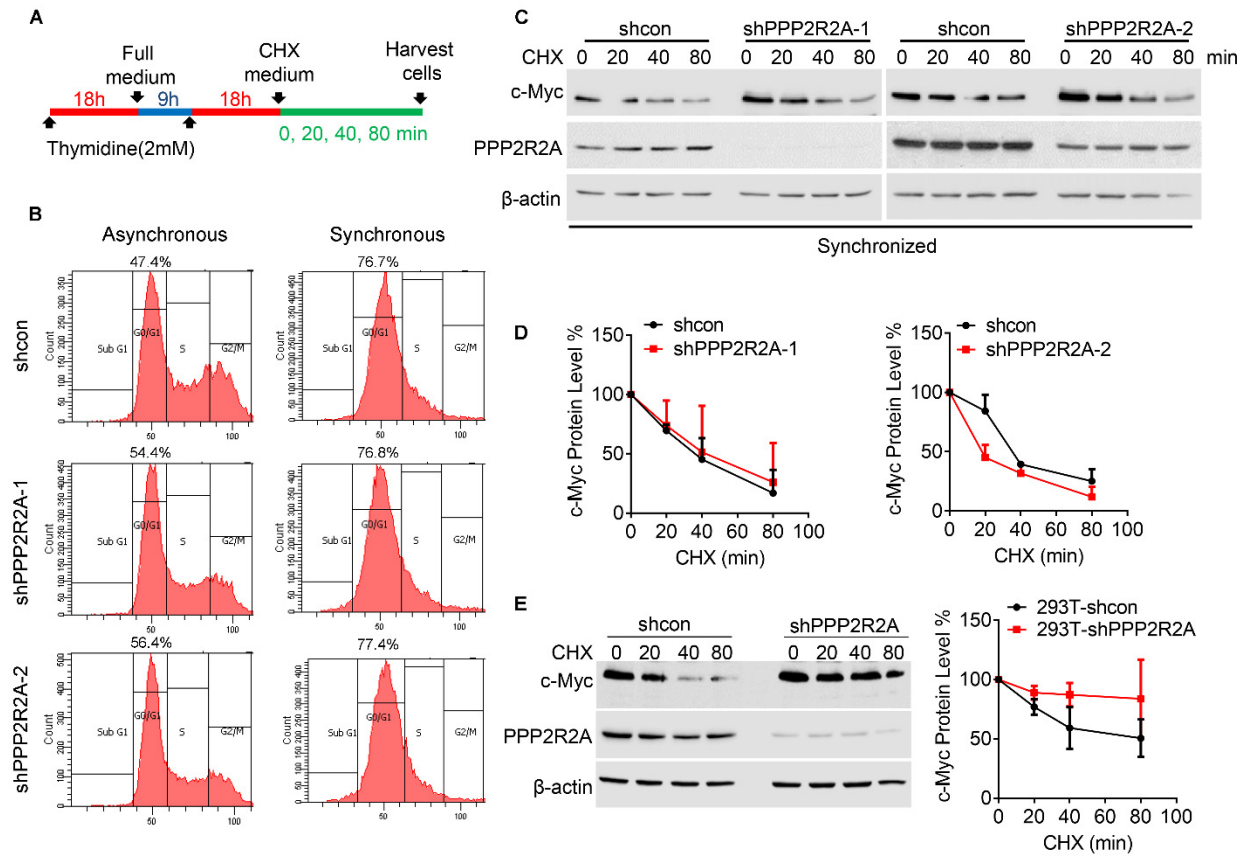

Supplementary Fig. S10. PPP2R2A knockdown has no effect on the half-life of c-Myc protein. (**A**) Schematic scale for double thymidine synchronization. (**B**) Cell cycle analysis of the DNA content of synchronized H1299 cells using double thymidine synchronization. (**C, D**) H1299 cells with or without PPP2R2A knockdown were synchronized according to the protocol indicated in **A**. c-Myc and PPP2R2A protein expression levels were determined using western blot; β-actin was used as loading control (**C**). c-Myc protein expression was quantified after three independent experiments (**D**). (**E**) PPP2R2A knockdown increased the half-life of c-Myc protein in HEK293T cells. HEK293T cells with or without PPP2R2A knockdown were synchronized in the HEK293T cells according to the protocol indicated in **A**. c-Myc and PPP2R2A protein expression levels were determined using western blot; β-actin was used as

loading control (left). c-Myc protein expression was quantified in three independent experiments (right). **D** and **E** (right panel) are presented as mean ± SEM of three independent experiments. Two-way ANOVA followed by Bonferroni post-tests was used for data analysis.

Supplementary Fig. S11

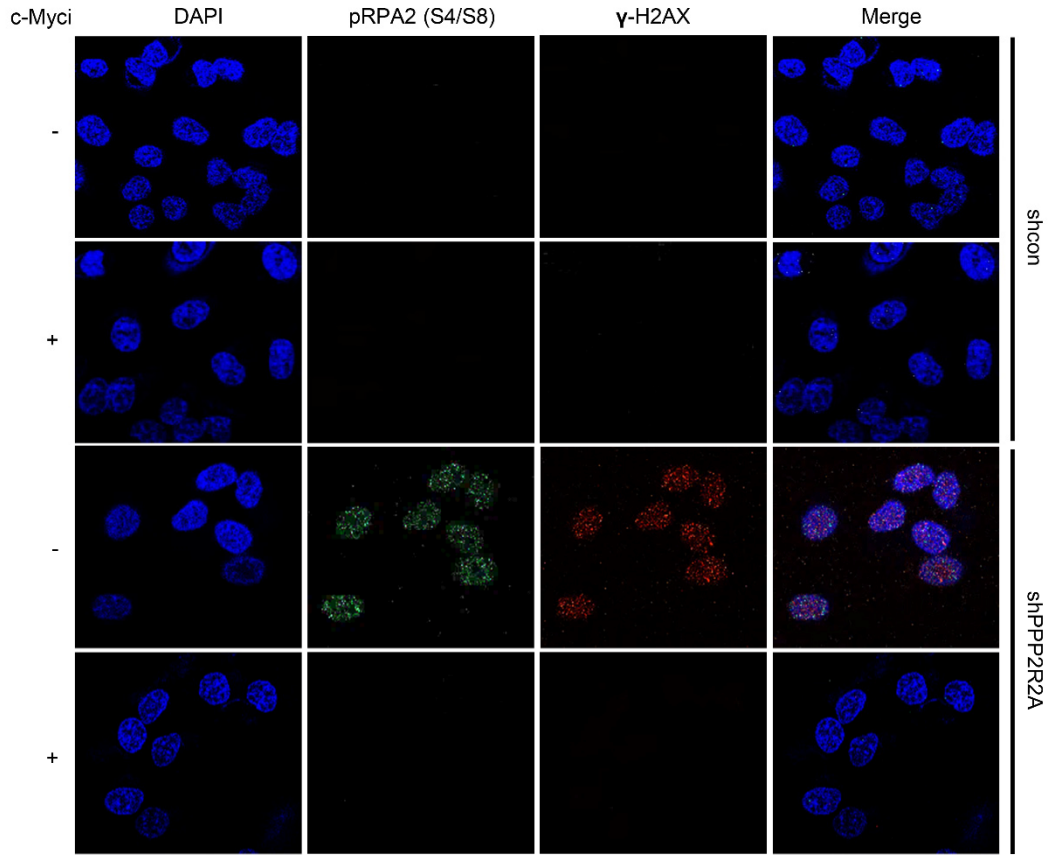

Supplementary Fig. S11. Representative immunofluorescence images of γ-H2AX and p-RPA2 (S4/S8) foci. H1299 control and H1299 PPP2R2A knockdown cells with or without c-Myc inhibitor 10058-F4 (20 μM) treatment. Scale bar: 100 μm.

Supplementary Fig. S12

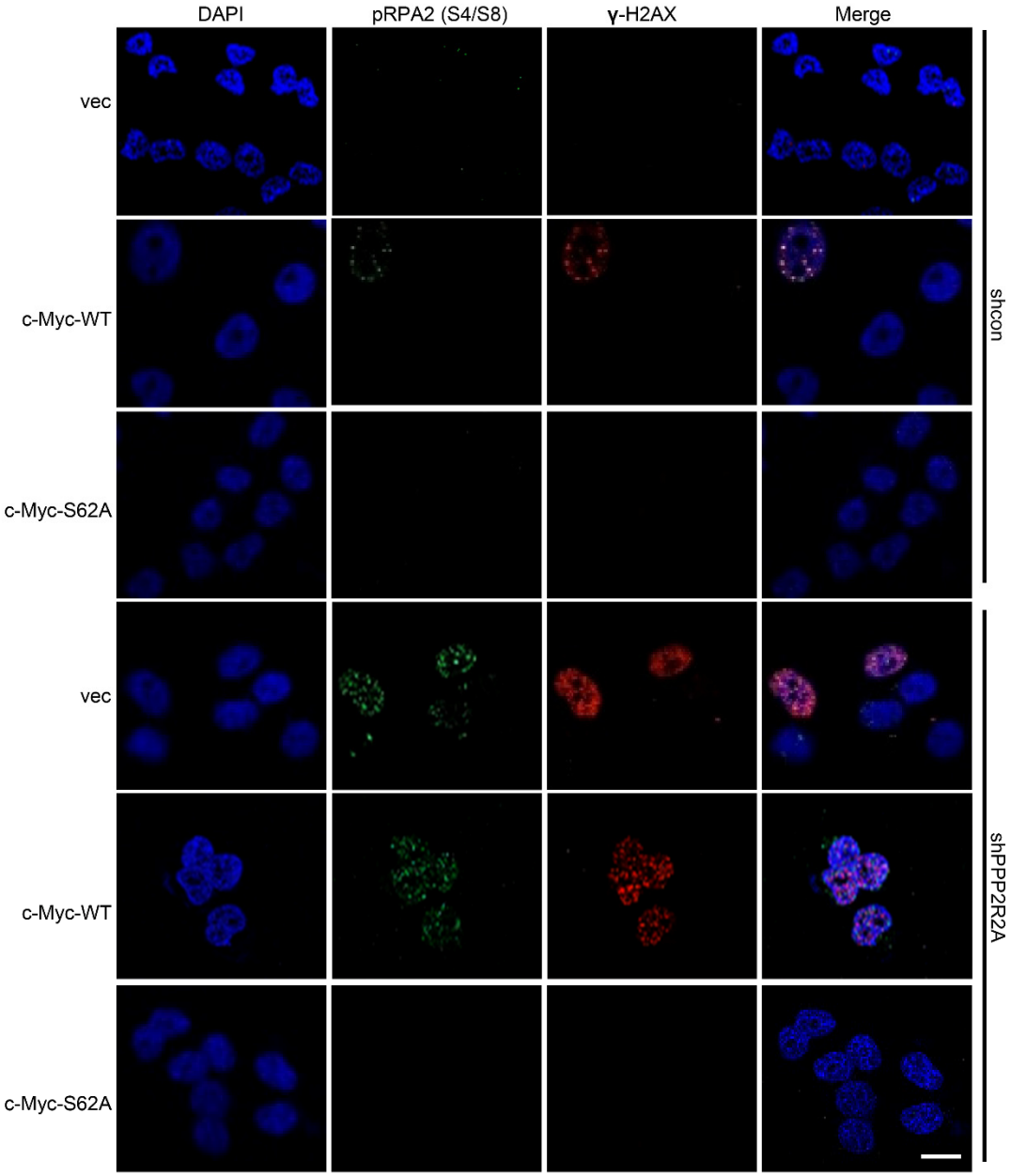

Supplementary Fig. S12. Representative immunofluorescence images of γ-H2AX and p-RPA2 (S4/S8) foci. H1299 cells with stable expression of vector, c-Myc-WT, or c-Myc-S62A in the presence or absence of PPP2R2A knockdown. Scale bar: 100 μm.

Supplementary Fig. S13

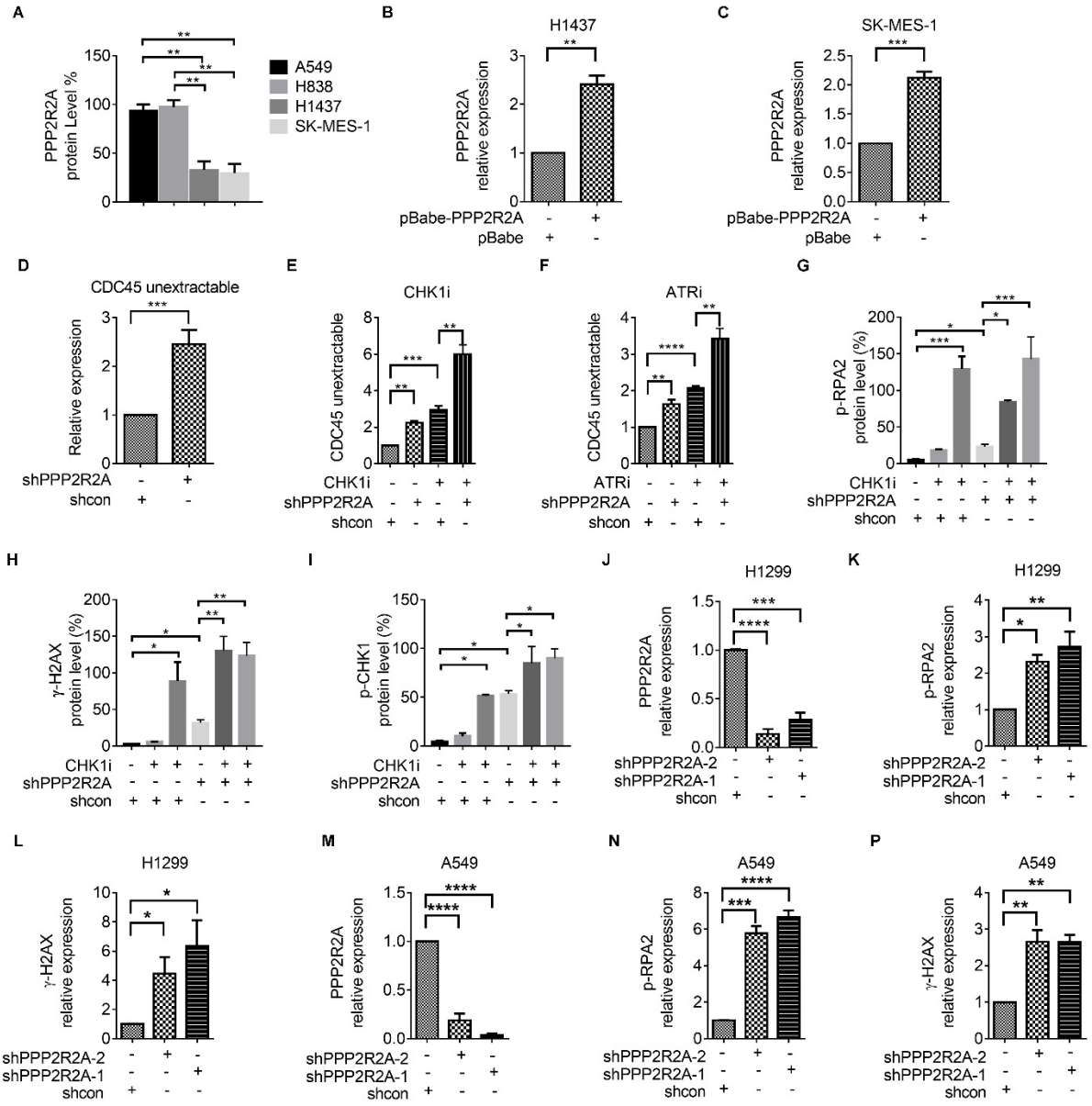

Supplementary Fig. S13. Densitometric quantitation of western blot results. Quantification of western blot results from the following figures: (**A**) Fig S3A; (**B-C**) Fig S3D; (**D**) Fig S4B; (**E-F**) Fig 3D; (**G-I**) Fig 4A; (**J-P**) Fig 5A. Data are shown as mean ± SEM of three replicates. Statistical analysis between two groups was performed by Student's *t* test (**B-D**). One-way ANOVA followed by Bonferroni post-test was used for the remaining data. **P* < 0.05, ***P* < 0.01,

***$P < 0.001$ and ****$P < 0.0001$.

Supplementary Fig. S14

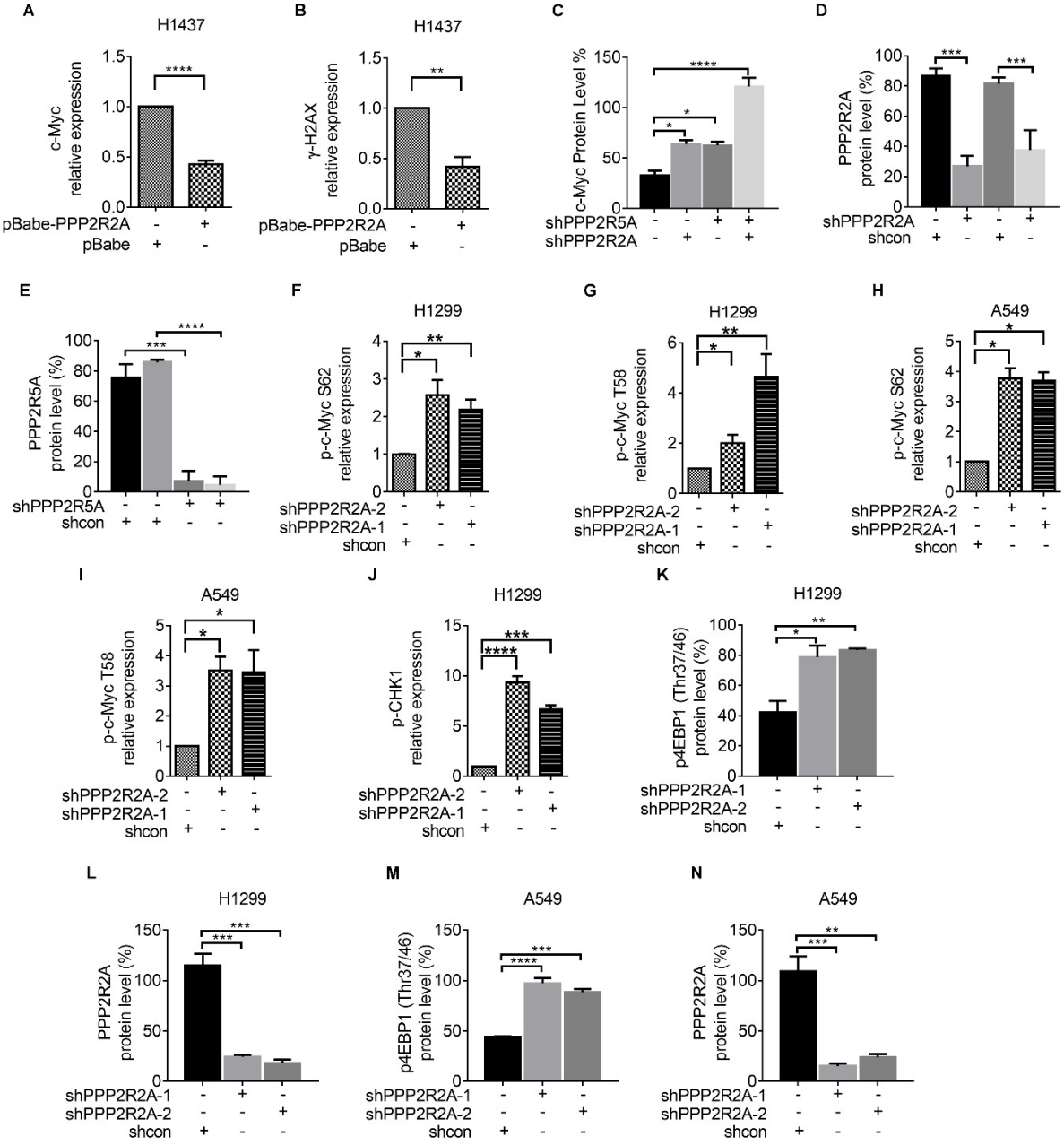

Supplementary Fig. S14. Densitometric quantitation of western blot results. Quantification of western blot results from the following figures: (**A-B**) Fig 5B; (**C-E**) Fig 5E; (**F-I**) Fig 6A; (**J**) Fig S6; (**K-N**) Fig 6E. *P < 0.05, **P < 0.01, ***P < 0.001 and ****P < 0.0001. Statistical analysis

between two groups was performed using the Student's *t* test (**A-B**). One-way ANOVA followed by Bonferroni post-test was used for the remaining data (**C-N**). Data are shown as mean ± SEM of three replicates.

Supplementary Fig. S15

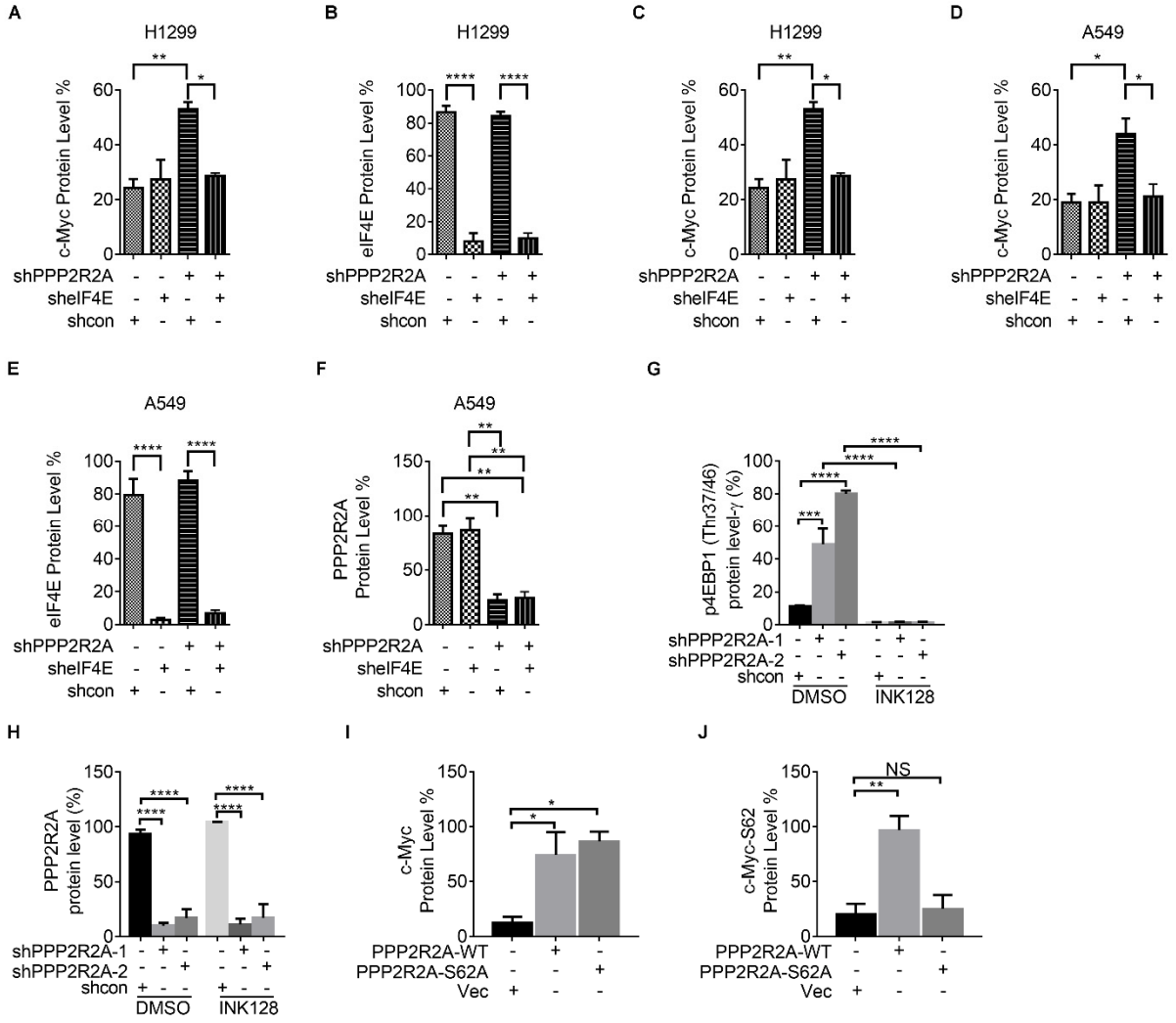

Supplementary Fig. S15. Densitometric quantitation of western blot results. Quantification of western blot results from the following figures: (**A-F**) Fig 6F; (**G-H**) Fig 6G; (**I-J**) Fig 7C. Data are shown as the mean ± SEM of three replicates. One-way ANOVA followed by Bonferroni post-tests was used for the data analysis. **P* < 0.05, ***P* < 0.01, ****P* < 0.001 and *****P* < 0.0001.